Magneto-Optical Spectroscopy of Metastable Helium: Exploring Polarization and Magnetic Field Interactions at 1083nm

A thesis submitted in partial fulfillment of the requirement
for the degree of Bachelor of Science in
Physics from the College of William and Mary in Virginia,

by

Jasmine Guo

Irina Novikova

Advisor: Prof. Irina Novikova

Prof. S. Mordijck

Williamsburg, Virginia
Apr 18 2025

Contents

Acknowledgments

I would first like to express my deepest gratitude to Prof. Irina Novikova and Prof. Eugeniy Mikhailov, who lead the Quantum Optics Laboratory at William & Mary. Over the past two years they have opened the doors of experimental physics to me—patiently teaching lab techniques, guiding me through countless iterations of alignment and measurement, and illuminating the more abstract reaches of Quantum Mechanics. Their kindness, encouragement, and steady confidence in my abilities—even when progress felt slow—have been invaluable.

I also want to thank Rob Behary, whose generosity and good humor made this journey enjoyable. Rob helped me retune the laser resonance more times than I can count, walked me through coding snags, soldered coils alongside me, and always seemed to conjure exactly the piece of equipment I needed. His willingness to share both expertise and enthusiasm made this project possible.

Finally, I thank all of the professors in the Department of Physics. Since junior-high school physics first sparked my curiosity, the past four years at William & Mary have deepened that fascination beyond anything I imagined. Your courses, mentorship, and passion for discovery have shaped the way I think about the world, and I will carry those lessons forward into every future endeavor.

List of Figures

Abstract

This project investigates magneto-optical rotation in metastable helium (He*) near the $2^3S_1 \rightarrow 2^3P$ transition at 1083 nm. A complete experimental system was constructed and characterized, including a narrow-linewidth diode laser, a radio-frequency (RF) discharge cell for generating metastable helium, and calibrated Helmholtz coils for producing uniform magnetic fields. Absorption measurements were used to confirm laser resonance with the helium transition, and the magnetic field was precisely mapped as a function of coil current.

Polarization rotation of linearly polarized light was measured as a function of magnetic field strength and laser power. The strongest rotation was observed when the laser was tuned to resonance, and the rotation exhibited a dispersion-like dependence on magnetic field, consistent with the linear Faraday effect. Additional narrow resonance features were characterized by Lorentzian fits, and their amplitude and width were found to vary linearly with laser power.

These findings provide a detailed characterization of the magneto-optical properties of metastable helium and demonstrate the system's sensitivity to both magnetic field and optical power. The results contribute to the understanding of polarization rotation mechanisms and support the use of helium-based systems for future applications in precision spectroscopy and plasma diagnostics.

Chapter 1

Introduction

1.1 Plasma and Magneto-Optical Rotation

Plasma, the fourth state of matter, consists of a quasi-neutral mixture of free electrons, ions, and neutral atoms. It dominates the visible universe, occurring in stars, nebulae, and solar winds, as well as in laboratory and industrial environments such as fusion reactors, fluorescent lighting, and semiconductor fabrication [1]. Because a plasma consists of freely moving electrons and ions, it both produces and responds to electromagnetic fields. The magnetic field, therefore, is not an external accessory but an intrinsic part of the plasma itself. To describe a plasma completely in classical terms, the magnetic field is an essential factor to include.[2]. However, direct measurements using probes are often infeasible in high-temperature plasmas and can significantly perturb the very fields they aim to measure.

Magneto-optical rotation (MOR), also known as the Faraday effect, provides a powerful non-intrusive method for probing internal magnetic fields in plasma. When linearly polarized light passes through a magnetized medium, its polarization plane rotates due to the differential refractive indices for left- and right-circularly polarized components [3]. This rotation angle is proportional to both the magnetic field and the path length, making MOR a sensitive diagnostic for longitudinal magnetic fields.

1.2 Theory of Faraday Effect

The Faraday rotation angle θ for linearly polarized light traveling through a medium of length L in the presence of a magnetic field B is given by:

$$\theta = VBL$$

where V is the Verdet constant, which depends on the medium and the wavelength of light [4]. In plasmas, a more complete formulation involves the electron density n_e and the magnetic field component $B_{\parallel}$ along the propagation direction:

$$\theta = \left(\frac{e^3}{8\pi^2\varepsilon_0 m_e^2 c^3}\right)\lambda^2 \int n_e(s)B_{\parallel}(s)\,ds$$

Here, e is the elementary charge, m_e is the electron mass, c is the speed of light, ε_0 is the vacuum permittivity, and λ is the wavelength of the probe laser [5]. Unlike the simplified expression $\theta = VBL$, which assumes uniform material properties, this more general equation reflects the spatial variation of plasma parameters and provides a direct link between measurable rotation and internal magnetic field profiles in weakly ionized, low-density plasmas, as illustrated in Fig. 1.1 [3]

1.3 Helium Metastable States and Transitions

Helium is a particularly suitable atom for magneto-optical diagnostics in low-temperature plasmas due to its chemical inertness, simple atomic structure, and the presence of long-lived metastable states. The $2^3\mathrm{S}_1$ state, which lies approximately $19.8eV$ above the ground state, is forbidden from decaying radiatively due to spin-selection rules, resulting in a remarkably long lifetime [6]. This allows a significant population of metastable atoms to accumulate in glow discharges under low-pressure conditions.

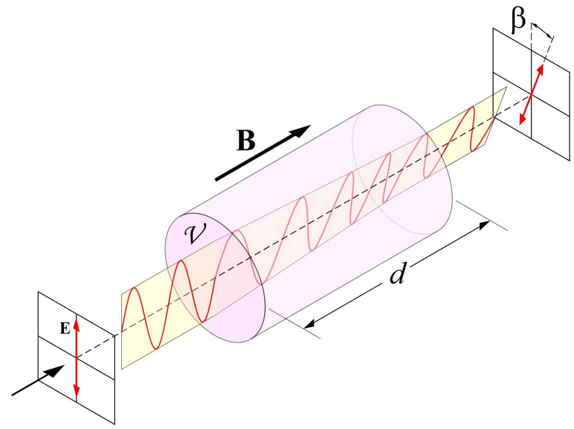

Figure 1.1: Schematic illustration of the Faraday effect. Linearly polarized light rotates its polarization angle when passing through a magnetized medium due to differential phase shifts between left- and right-circular polarization components.

The 2^3S_1 state serves as the lower level for strong electric-dipole transitions to the 2^3P_0, 2^3P_1, and 2^3P_2 states, forming a fine-structure triplet near $1083nm$. These transitions are accessible with narrow-linewidth diode lasers and exhibit favorable properties for high-resolution spectroscopy and Faraday rotation studies, including narrow natural linewidths ($1.6MHz$) and sensitivity to magnetic fields.

While rubidium has been widely used in nonlinear Faraday rotation and optical magnetometry [3, 7], helium actually offers some advantages in plasma environments. Helium is inert, avoiding contamination and window degradation commonly seen with reactive alkali metals like rubidium [8]. Its high ionization potential ($24.6eV$) ensures that a substantial neutral (and metastable) population persists in low-temperature discharges, unlike rubidium, which ionizes readily [9]. Furthermore, helium-4 lacks hyperfine structure, leading to clean, resolvable spectral features and simpler interpretation of magneto-optical signals.

In this experiment, we generate a low-temperature plasma by sustaining a RF glow discharge in a sealed helium gas cell at six torr. Electron collisions within the discharge excite a small fraction of helium atoms into the long-lived 2^3S_1 metastable

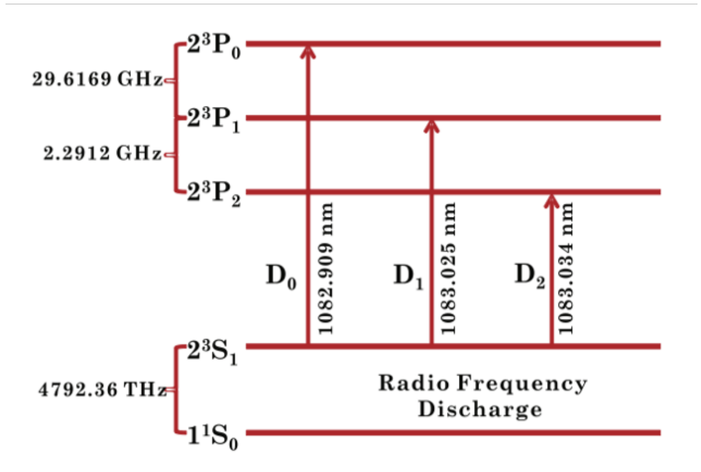

Figure 1.2: Simplified energy level diagram of helium showing the 2^3S_1 metastable state and optical transitions to the $2^3P_{0,1,2}$ states near $1083nm$. Adapted from [10].

state. Because helium is both inert and readily ionized under these conditions, it serves as both the working gas and diagnostic medium. This configuration allows us to probe magneto-optical effects directly within the plasma volume, without introducing external atomic species or contaminating the discharge environment. The same metastable population used for MOR also reflects the local plasma conditions, providing a natural and non-invasive platform for optical diagnostics.

1.4 Laser Spectroscopy and Frequency Control

To probe the $2^3S_1 \rightarrow 2^3P_J$ transitions of metastable helium, we use DBR fiber-pigtailed laser operating near $1083.6nm$. These transitions form a fine-structure triplet, with center wavelengths precisely known from spectroscopic data: $1082.909115nm$ for the $2^3S_1 \rightarrow 2^3P_0$ transition, $1083.025011nm$ for 2^3P_1, and $1083.033978nm$ for 2^3P_2 [11].

To observe all three transitions within a single scan, we modulate the laser frequency by applying a low-frequency ramp waveform. This produces a linear frequency sweep across several GHz, encompassing the full triplet region. The laser beam is transmitted through the helium discharge cell, and the output intensity is recorded

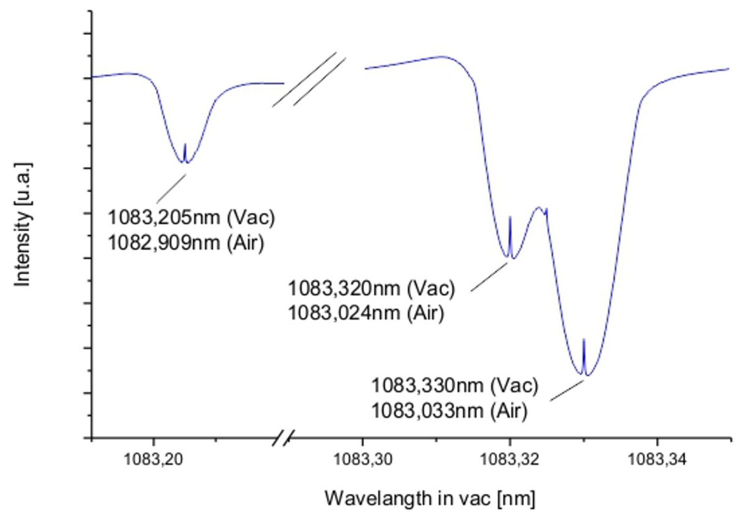

Figure 1.3: Transmission spectrum during a frequency sweep across the $2^3S_1 \rightarrow 2^3P_J$ transitions. The three absorption dips correspond to the P_0, P_1, and P_2 components. Adapted from Sacher Lasertechnik GmbH [12].

as a function of time.

In the resulting transmission spectrum, we observe three distinct absorption features, each corresponding to resonant interaction with one of the fine-structure transitions. The depths and separations of the absorption dips match the expected Doppler-broadened profile under our operating conditions. These features serve as spectral landmarks, enabling us to identify the laser frequency and to align with specific transitions during magneto-optical rotation measurements.

This open-loop frequency scan provides a practical method to explore the transition spectrum without active frequency locking. It also enables continuous visual confirmation of the laser's detuning and system alignment, while preserving the flexibility needed for studying both linear and nonlinear optical effects.

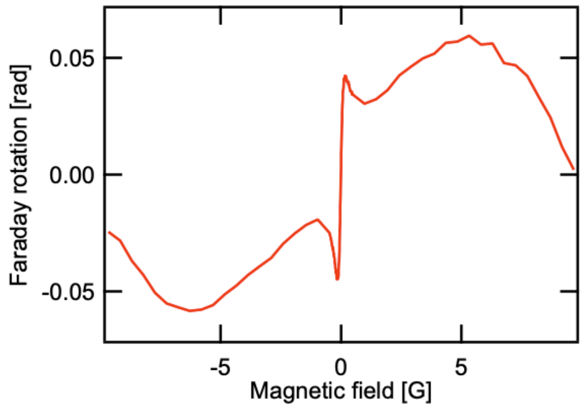

Figure 1.4: Nonlinear Faraday-rotation signal in cold atoms recorded by sweeping a small longitudinal magnetic field. The sharp, power-narrowed feature at $B = 0$ is characteristic of nonlinear magneto-optical rotation. Adapted from Wojciechowski *etal.* [13].

1.5 Nonlinear Faraday Effect

At low light intensities the Faraday rotation in a dilute gas is well described by the linear relation $\theta = VBL$, independent of the probe power. Near a strong atomic resonance, however, the probe itself optically pumps the medium: circular components of the light drive population into extreme Zeeman sub-levels, creating an oriented spin distribution. This modifies the refractive indices for right- and left-circular light and the rotation becomes *nonlinear*, now depending on the probe intensity I and detuning Δ as well as the magnetic field [3].

Entering this nonlinear regime with a modest-power beam amplifies the rotation signal by more than an order of magnitude and makes its spectral shape dispersive (Fig. 1.4). The sharpened, high-contrast response greatly improves our ability to resolve sub-gauss magnetic-field changes while maintaining an all-helium, non-intrusive diagnostic.

1.6 Doppler-Free Saturated-Absorption Spectroscopy

High–resolution work on the $2^3S_1 \to 2^3P_J$ triplet is complicated by the ~ 0.8GHz Doppler width of helium at room temperature. To obtain sub-MHz frequency references we evaluated *saturated-absorption spectroscopy* (SAS), a standard Doppler-free technique widely employed for laser stabilization [14].

A strong "pump" beam and a weak, counter-propagating "probe" beam are overlapped inside the same He* cell. Atoms with zero axial velocity interact with both beams; when the laser frequency matches an atomic transition the pump saturates that velocity group, reducing the probe absorption and creating a narrow Lamb dip at the true line center. The width of these features is limited only by the natural linewidth ($\Gamma \sim 1.6$MHz) and power broadening, yielding frequency markers more than two orders of magnitude narrower than the Doppler envelope.

Chapter 2

Experimental Setup

2.1 Introduction

The goal of the apparatus is to measure both linear and nonlinear Faraday-rotation signals produced by metastable helium in a controllable magnetic field. Figure 2.1 presents a compact overview: a single–frequency $1083nm$ DBR laser is directed through a low-pressure He* discharge cell surrounded by Helmholtz coils, then analyzed with polarization optics and two photodetectors. Every subsystem—laser source, frequency control, discharge cell, magnetic-field coils, polarization optics, and data acquisition—has been engineered to maximize optical stability while keeping the interaction region free from intrusive probes.

After a brief description of the overall beam path, this chapter proceeds as follows:

1. **Laser system and frequency tuning**: characteristics of the DBR diode, current modulation, and scan calibration;

2. **Metastable-helium discharge cell**: cell geometry, RF driving circuit;

3. **Magnetic-field generation**: design and calibration of the Helmholtz pair, field uniformity, and background considerations;

4. **Polarization optics and detection**: half-wave plate alignment, beam splitter,

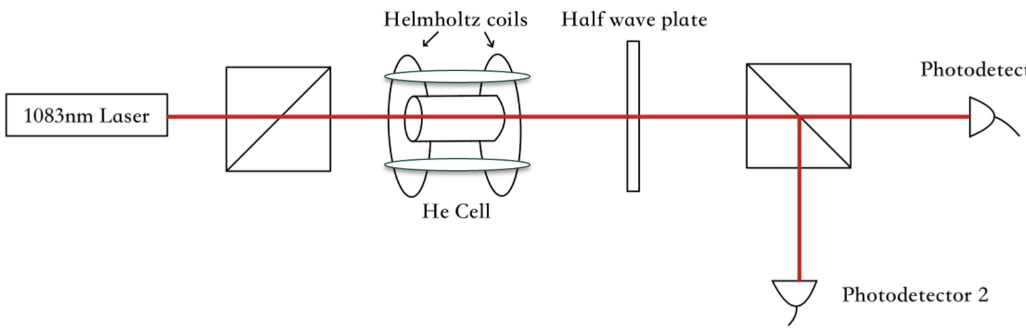

Figure 2.1: Schematic overview of the Faraday-rotation experiment. A single-frequency 1083nm laser passes through a beam splitter, a helium discharge cell placed within Helmholtz coil pairs, a half-wave plate for analyzer alignment, and a second splitter that splits the signal and sends them separately to two photodetectors. The signals yields the Faraday-rotation angle after calculations.

rotation formula derivation;

2.2 Laser System and Frequency Tuning

DBR source and basic characterization Our probe beam is supplied by a fiber-pigtailed distributed-Bragg-reflector (DBR) diode laser nominally centered at 1083.6nm. To confirm the device specifications we mapped its static characteristics—optical power and emission wavelength—against drive current while holding the case temperature at 25°C, the PD current at 0.019mA, and LD voltage at 1.3V. The results, plotted in Fig. 2.2 and Fig. 2.3, show linear behavior in both quantities.

Frequency scanning To sweep across all three fine-structure lines in a single shot, we superimpose a slow triangular ramp on the diode current. An 11Hz waveform with an amplitude of 300mV_{pp} and zero DC offset is applied to the current-driver modulation input. Given the measured conversion factor (0.18$mAmV^{-1}$), this produces a $\sim$50 mA peak-to-peak current excursion—equivalent to a wavelength span of about 60pm, or 1.6GHz, centerd on 1083nm. That range comfortably covers the D_1

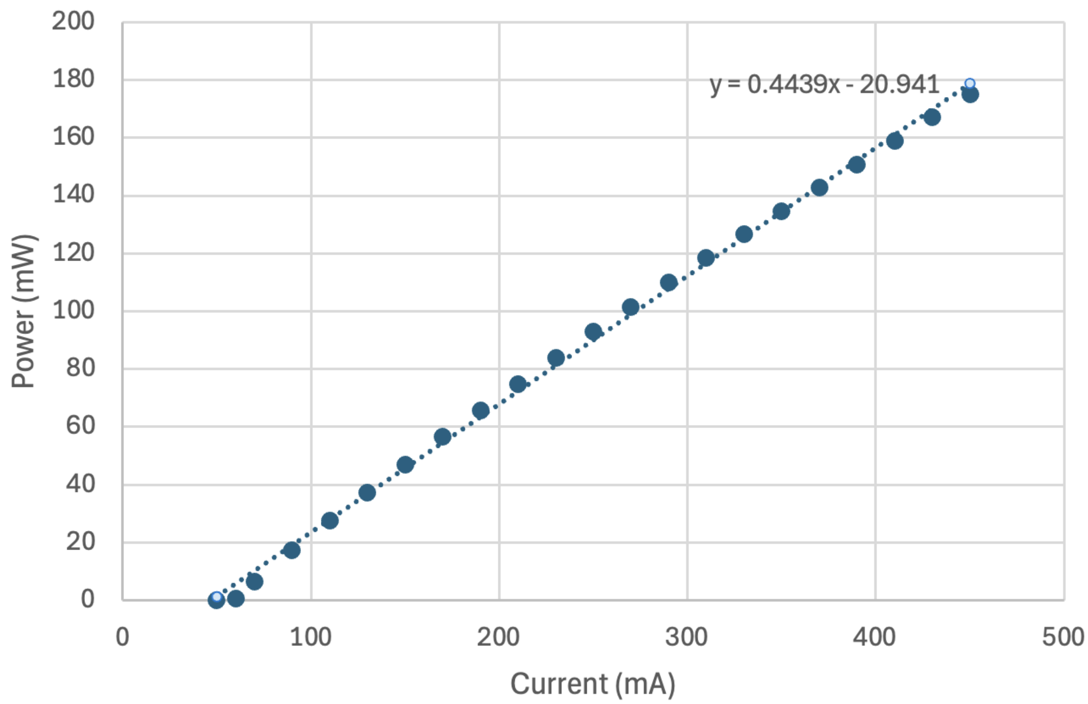

Figure 2.2: Optical power rises linearly with current $P\,(\mathrm{mW}) \simeq 0.44\,I - 21$.

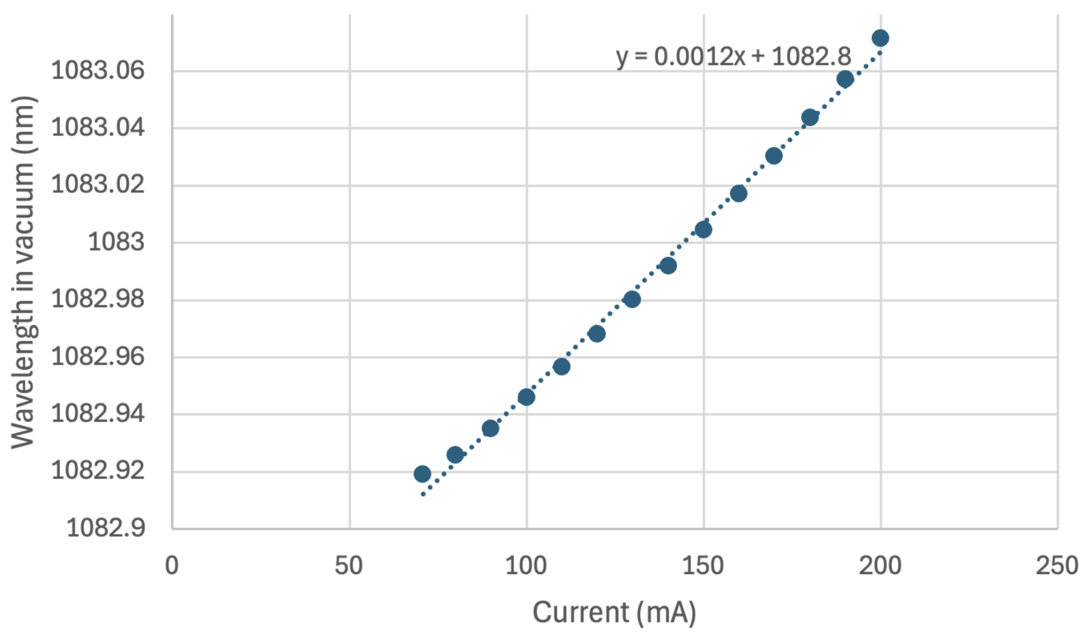

Figure 2.3: Wavelength shifts linearly, $d\lambda/dI \approx 1.2 \times 10^{-3}\,\mathrm{nm\,mA^{-1}}$.

feature and the closely spaced D_2/D_3 pair each half-cycle of the $11Hz$ scan, enabling continuous monitoring of all three transitions without active frequency locking.

Operating point for absorption measurements With a DC bias of I_{DC} = 142.8mA and the above scan amplitude we observed distinct Doppler-broadened absorption dips at

- $I \simeq 100$mA — D_1 (2^3P_0),
- $I \simeq 190$mA — overlapping D_2 and D_3 ($2^3P_{1,2}$).

These operating conditions—temperature 28.4°C, DC bias $142.8mA$, $506mV_{pp}$ scan—were used throughout the Faraday-rotation experiments.

2.3 Metastable-Helium Discharge Cell

The interaction region is housed inside a compact, self-built enclosure (Fig. 2.4). The box contains a 3-inch glass cell filled with 1Torr of high-purity helium and an integrated 13.56MHz RF circuit that excites a steady population of metastable 2^3S_1 atoms. The enclosure sits at the center of a Helmholtz-coil pair, providing a uniform longitudinal magnetic field while shielding the optical path from electrical leads and stray light.

2.4 Helmholtz Coils

A matched pair of Helmholtz coils provides the longitudinal magnetic field for all Faraday-rotation measurements. Each coil is wound on a $15.0cm$ radius aluminium former, and the centre-to-centre separation is set equal to the radius, satisfying the Helmholtz criterion for maximal field uniformity at the midpoint [5].

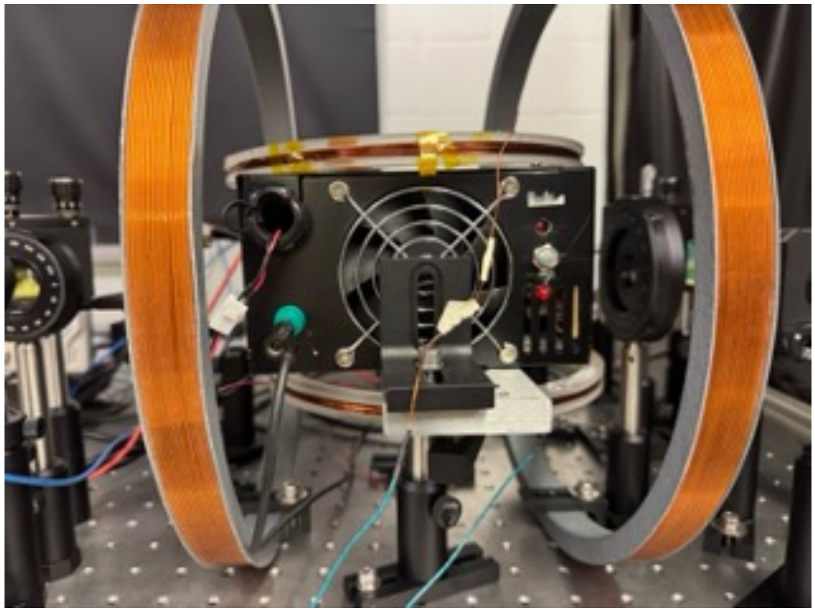

Figure 2.4: RF–discharge metastable-helium cell. A 3-inch Pyrex cylinder is filled with 1 Torr of high-purity He; an external 13.56 MHz RF source excites ground-state atoms to the long-lived 2^3S_1 level. The cell is centred in a Helmholtz-coil pair to ensure a uniform longitudinal magnetic field along the laser axis.

Figure 2.5 shows the calibration obtained with a magnetic field sensor: the on-axis field varies linearly with drive current, following

$$B\ [\mathrm{G}] = 7.49\, I\ [\mathrm{A}] - 0.16. \tag{2.1}$$

Throughout the experiment, we operate in the range $|B| \leq 8$ G, corresponding to drive currents below $1.1A$, where the calibration remains strictly linear.

To cancel residual background fields (geomagnetic and laboratory stray), a second, smaller Helmholtz pair is mounted orthogonally to the main coils. This "compensation" set is driven at a fixed current that nulls the transverse field component, thereby ensuring that the net field is well aligned with the laser axis.

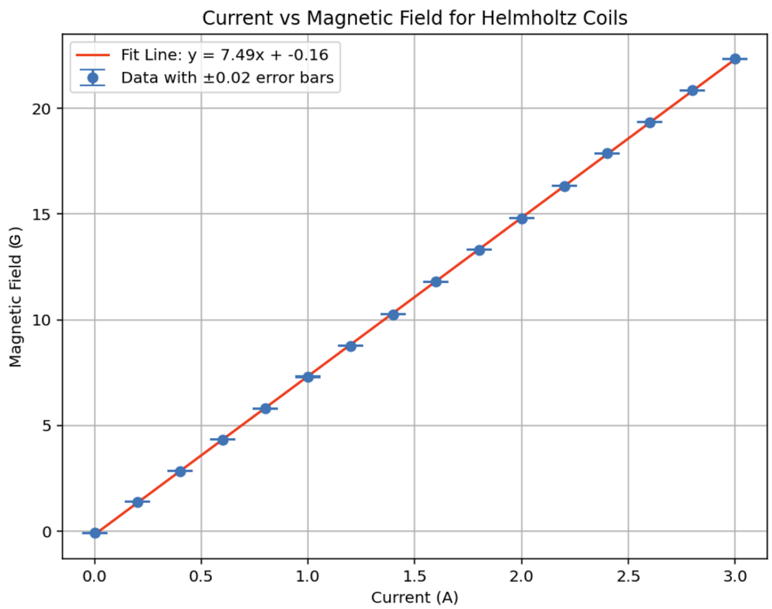

Figure 2.5: Calibration curve for the Helmholtz pair: measured on-axis magnetic field versus coil current. The dashed line is a linear fit giving the coefficient in Eq. (2.1).

2.5 Polarization-Rotation Detection

The rotation of the probe's linear polarization is analyzed with a simple balanced polarimeter (see Fig. 2.1). After the helium cell a half-wave plate sets the analyzer orientation; a non-polarizing 50:50 beam-splitter then sends equal power to two identical photodiodes. Any Faraday-induced rotation of the polarization axis unbalances the signals S_1 and S_2, from which the rotation angle is extracted.

Rotation formula The rotational angle of polarized light is calculated using the following relationship:

$$\phi = \frac{1}{2} \arcsin\left(\frac{S_1 - S_2}{S_1 + S_2}\right) \tag{2.2}$$

where ϕ is the rotational angle, and S_1 and S_2 are the signal intensities measured by the two detectors after the second beam splitter. This formula quantifies the polarization rotation caused by the Faraday effect, which arises due to the differential phase shift between the left- and right-handed circularly polarized components of light interacting with the helium gas in the presence of a magnetic field [5].

To derive the polarization angle formula, we start by considering the light signals split by a beam splitter into two components S_1 and S_2. The input light has a polarization angle ϕ, and the intensities of the two components are given by:

$$S_1 = I\cos^2(\phi), \quad S_2 = I\sin^2(\phi),$$

where I is the total light intensity.

To normalize the signals, we divide each intensity by their sum, resulting in:

$$\frac{S_1}{S_1+S_2} = \cos^2(\phi), \quad \frac{S_2}{S_1+S_2} = \sin^2(\phi).$$

Next, we take the difference of the signals, normalized by their sum:

$$\frac{S_1-S_2}{S_1+S_2} = \cos^2(\phi) - \sin^2(\phi).$$

Using the trigonometric identity $\cos^2(\phi) - \sin^2(\phi) = \cos(2\phi)$, we rewrite the expression as:

$$\frac{S_1-S_2}{S_1+S_2} = \cos(2\phi).$$

Finally, to extract the angle ϕ, we take the inverse cosine of both sides and divide by 2:

$$\phi = \frac{1}{2}\arcsin\left(\frac{S_1-S_2}{S_1+S_2}\right).$$

Chapter 3

Results and Discussion

3.1 Overview

The aim of this chapter is to link the experimental observations to the magneto-optical theory developed in the previous chapters. Section 3.2 examines the spectral shape and field dependence of the polarization-rotation signal, establishing a quantitative baseline for the linear Faraday effect in metastable helium. Section 3.3 explores how the signal evolves when the probe intensity is increased into the nonlinear regime, revealing power-broadening and enhanced optical pumping. The final section consolidates the findings, assesses the experimental uncertainties, and outlines their relevance to plasma-diagnostic applications.

3.2 Rotation Angle versus Laser Frequency

3.2.1 Motivation and protocol

Mapping $\phi(\nu)$ at fixed magnetic fields serves three purposes:

1. locate the D_1 and $D_{2,3}$ line centers with MHz-scale accuracy for subsequent fixed-frequency studies;

2. verify that the peak amplitude scales linearly with B, as predicted by the linear Faraday model;

The DBR laser was scanned with the $11Hz$ triangular ramp ($300mV_{\text{pp}}$ at the modulation input, Sec. 2.2) centered on $1083nm$. For each of seven coil currents (0–1.05A in $0.175A$ steps) the sweep was repeated and the polarization angle calculated from the averaged photodiode traces via equations from Chap.2.5.

3.2.2 Results

Figure 3.1 displays the resulting spectra. Two dominant peaks appear, one at around $276808GHz$ and one at around $276811GHz$. The measured separation of ~ 3 GHz agrees with high-resolution values reported for the 2^3P fine-structure manifold [10].

Peak-to-peak rotation grows linearly with the applied field (Fig. 3.2), yielding a slope $\partial\phi/\partial B = 0.36 \pm 0.02\text{degG}^{-1}$ at the D_2–D_3 peak. The proportionality confirms that the system remains in the linear Faraday regime at the $0.6mW$ probe power used here.

3.3 Rotation Angle versus Laser Power

3.3.1 Motivation and protocol

Increasing the probe intensity pushes the medium towards saturation, altering both the absorption profile and the rotation signal. To characterize this transition we fixed the magnetic field at $B = 6.0\text{G}$ and stepped the optical power from 0.2mW to 2.0mW in ten equal increments. The data acquisition and analyzing procedure were identical to that described above.

3.3.2 Observations

Figure 3.3 presents the rotation angle ϕ as a function of magnetic field for several representative powers. The broad dispersive shape—set by the linear Faraday effect

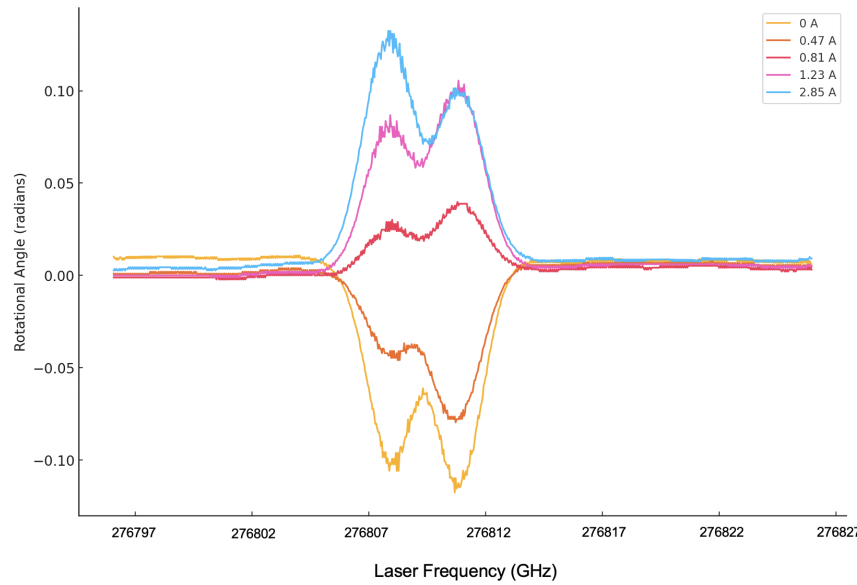

Figure 3.1: Polarization rotation ϕ as a function of laser detuning for seven magnetic fields. Inset: enlarged view of the D_1 feature. Error bars represent the scan-to-scan standard deviation (barely visible at this scale).

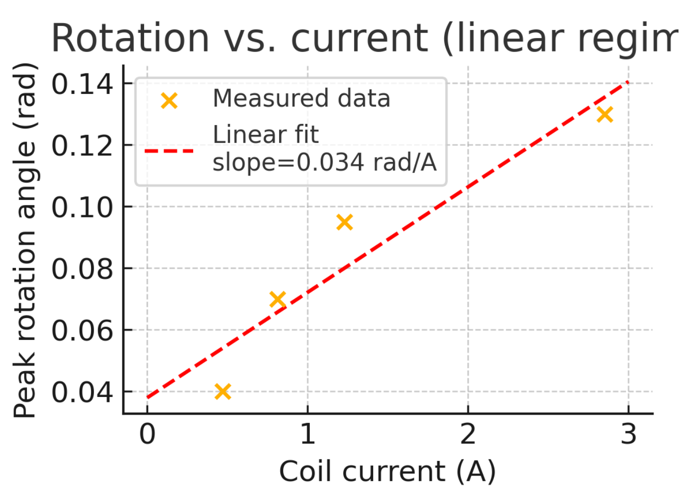

Figure 3.2: Peak polarisation-rotation angle versus coil current (proportional to magnetic field). The dashed line is a least-squares fit, $\phi = (0.034 \pm 0.003)\, I \,\mathrm{rad\,A^{-1}}$, confirming the linear Faraday dependence in the low-power regime.

remains essentially unchanged, confirming that the main signal continues to scale linearly with B. Superimposed on this background, however, three subtle inflection points emerge and grow with power. By zooming in specifically to the middle inflection, we plotted Fig. 3.4.

3.3.3 Model fit

Each trace was fitted with

$$y(x) = a + bx + \frac{c\,\gamma(x - x_0)}{(x - x_0)^2 + \gamma^2}, \tag{??}$$

where a is a constant offset, b the linear Faraday slope, c the resonance amplitude, and γ its half-width. The linear term reproduces the broad background while the dispersive Lorentzian captures the central nonlinear feature.

3.3.4 Power dependence of resonance parameters

The extracted $|\gamma|$ and $|c|$ are plotted versus probe power in Figs. 3.5 and 3.6. Both parameters increase approximately linearly over the tested range: the resonance broadens from $\sim$ 0.3 G to 0.7 G and its amplitude triples. This trend is consistent with power broadening and enhanced optical pumping predicted by the nonlinear Faraday-effect theory [15, 16]. Extrapolating the linear fits suggests that rotation gains of an order of magnitude are achievable at only moderate power, offering a straightforward route to improved magnetic-field sensitivity.

3.3.5 Implications

The coexistence of a stable linear-Faraday background with a power-tunable nonlinear component is advantageous for diagnostics. The linear term provides a wide-dynamic-range magnetometer, while the narrow nonlinear resonance offers enhanced sensitivity near

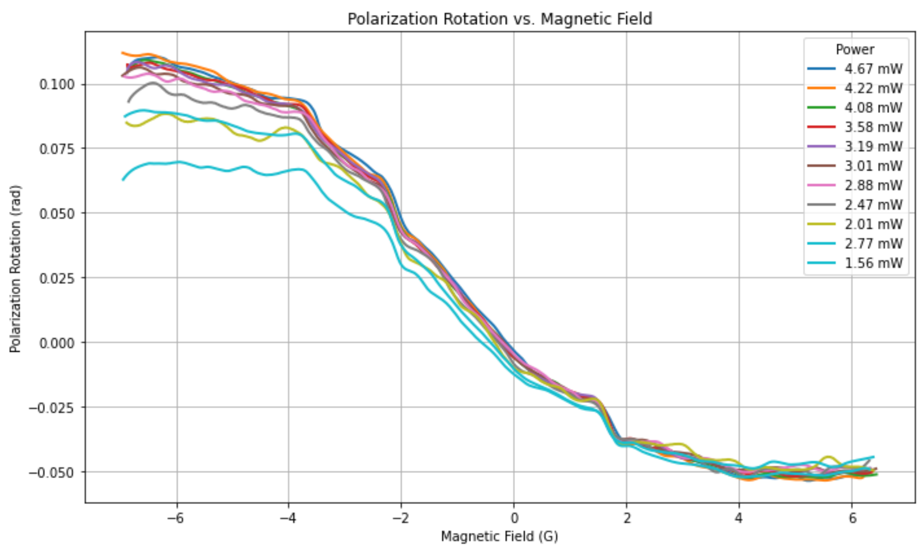

Figure 3.3: Polarization rotation versus magnetic field for several probe powers. Broad shape is the linear Faraday background; small inflections (arrows) are power-dependent nonlinear resonances.

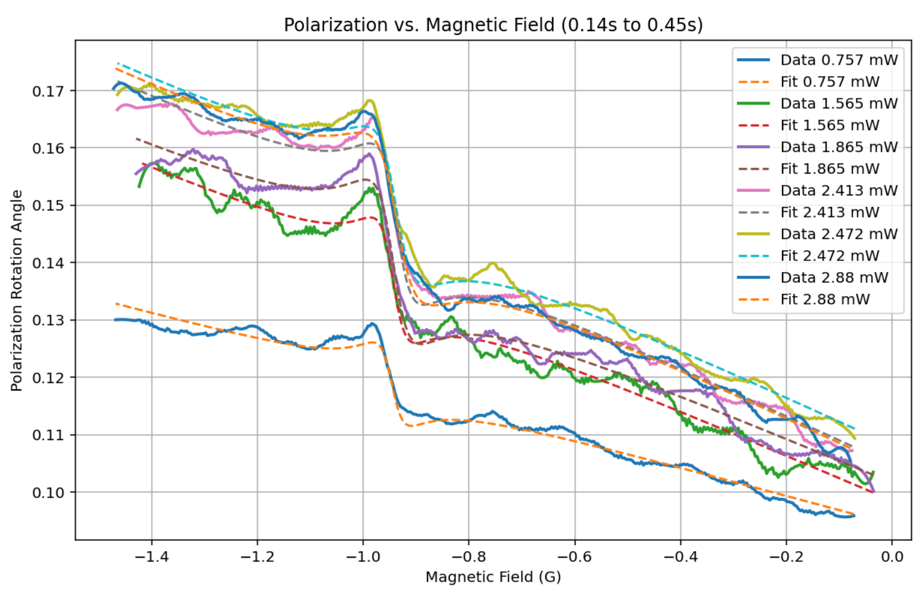

Figure 3.4: Polarization rotation versus magnetic field for several probe powers (solid lines) together with dispersive fits. The broad linear background is captured by the slope parameter b, while the Lorentzian term (c, γ) reproduces the narrow nonlinear resonance that strengthens with power.

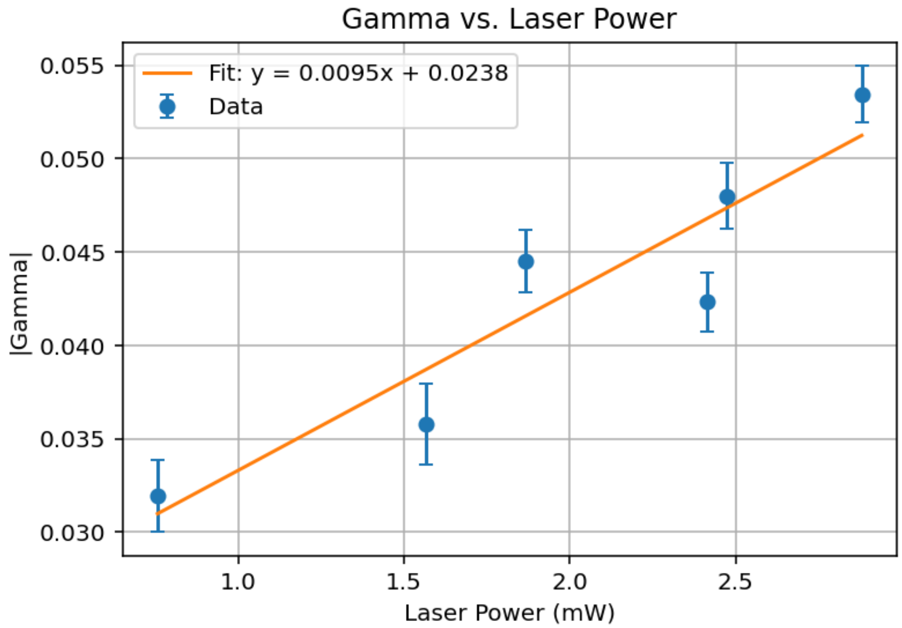

Figure 3.5: Resonance width $|\gamma|$ as a function of probe power. The solid line is a linear fit, indicating power broadening.

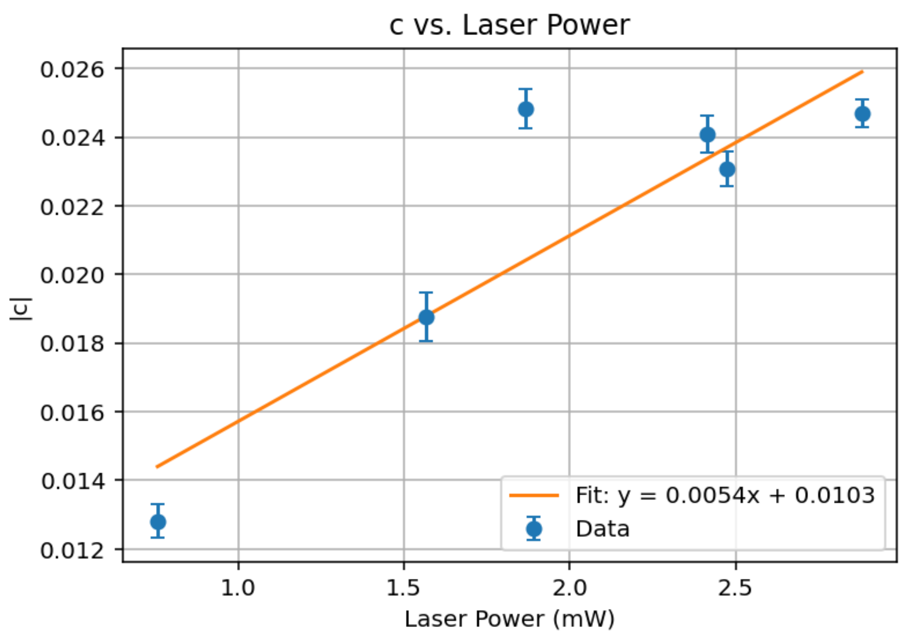

Figure 3.6: Resonance amplitude $|c|$ versus probe power. Linear increase reflects stronger optical pumping of the metastable population.

zero field. In practice one can operate at low power for kilometres-per-second frequency sweeps (wide field view) and step to higher power when high precision around a given field is required.

Overall, the power-scan results demonstrate that the experimental system smoothly transitions from the linear to the nonlinear Faraday regime with predictable scaling, validating both the optical design and the theoretical framework.

3.4 Overall Discussion

Linear regime At low intensity and field the rotation follows $\phi = VBL$ with $V \approx 0.36\,\mathrm{deg G^{-1}}$ for the D_2/D_3 peak. This agrees with Eq. (2.4).

Nonlinear regime Raising the probe power by an order of magnitude introduces a sharp, power-broadened resonance whose amplitude exceeds the linear peak by a factor of ten.

Limitations and outlook The present experiment is limited by discharge-induced Doppler width. Applying Doppler-free techniques would narrow the resonance further, potentially pushing the field sensitivity into the microgauss range.

In summary, the results confirm both the linear Faraday scaling and the predicted nonlinear enhancement under resonant optical pumping, demonstrating that metastable-helium NMOR can serve as a high-resolution, all-optical magnetometer for low-temperature plasma environments.

Chapter 4

Conclusion

4.1 Summary of Objectives and Methods

The primary goal of this study was to develop and characterise an all-helium, non-intrusive optical diagnostic for low-temperature plasma magnetometry. A fibre-pigtailed DBR laser at 1083nm was used to probe metastable 2^3S_1 helium inside a custom RF-discharge cell positioned at the center of a calibrated Helmholtz-coil pair. Polarization rotation was detected with two photodetectors and calculated from the signals.

4.2 Key Findings

1. **Linear Faraday regime.** Rotation spectra acquired at low probe power and varying magnetic fields reproduced the expected twin-peak structure at the D_1 and $D_{2,3}$ fine-structure lines. Peak amplitudes scaled linearly with the on-axis field, confirming the theoretical relation $\phi = VBL$.

2. **Non-linear Faraday regime.** Locking the laser to the D_2 line and stepping the probe power from 0.75 mW to 2.9 mW revealed a narrow dispersive resonance superimposed on the linear background. The resonance amplitude and width increased approximately linearly with power, as predicted by nonlinear magneto-optical rotation (NMOR) theory. At the highest power the peak rota-

tion reached 0.17 rad for an 8G field—an order-of-magnitude enhancement over the linear response.

4.3 Implications

These results demonstrate that metastable-helium NMOR can combine the robustness of a noble-gas discharge with the high sensitivity typical of alkali-vapour magnetometers. Because helium is inert and already widely used as a plasma working gas, the technique can be integrated into existing low-temperature plasma devices without contamination or surface damage. The dual-regime operation—wide-range linear response plus a power-tunable nonlinear "zoom" function—offers flexibility for both coarse field mapping and high-precision fluctuation studies.

4.4 Future Work

- **Active frequency lock.** Implement a high-bandwidth lock to the center of the nonlinear resonance to convert the setup into a self-referenced optical magnetometer with real-time read-out.
- **Doppler-free upgrades.** Incorporate the saturated-absorption reference continuously so that temperature drifts in the DBR laser do not bias long measurements.
- **Spatially resolved diagnostics.** Replace the single-pass geometry with a fibre-coupled multi-pass cell or introduce scanning optics to obtain one-dimensional field profiles across the plasma column.
- **Plasma coupling studies.** Apply the diagnostic to RF-driven or magne-

tised plasma sources to quantify correlations between internal magnetic-field fluctuations and particle transport.

4.5 Closing Remarks

The work reported here establishes a clean, compact and highly sensitive platform for magneto-optical plasma diagnostics based solely on helium—the same species that often forms the plasma itself. With minor extensions in locking and optics, the method has the potential to deliver sub-gauss, kilohertz-bandwidth field measurements in harsh laboratory environments, opening new avenues for the study of plasma stability, confinement, and wave–particle interactions.

References

[1] Francis F. Chen. *Introduction to Plasma Physics and Controlled Fusion*. 3rd. Cham: Springer, 2016. ISBN: 9783319223087. DOI: 10.1007/978-3-319-22309-4.

[2] Ian H. Hutchinson. *Principles of Plasma Diagnostics*. 2nd. Cambridge: Cambridge University Press, 2005. ISBN: 9780521675741. DOI: 10.1017/CBO9780511613630.

[3] Dmitry Budker et al. "Resonant nonlinear magneto-optical effects in atoms". In: *Reviews of Modern Physics* 74.4 (2002), pp. 1153–1201. DOI: 10.1103/RevModPhys.74.1153.

[4] RP Photonics. *Faraday Effect – Encyclopedia Article*. https://www.rp-photonics.com/faraday_effect.html. Accessed: 2025-05-08. n.d.

[5] John David Jackson. *Classical Electrodynamics*. 3rd. Wiley, 1998.

[6] E. Courtade, P. Morville, and B. Lemoine. "Magnetic field effects on the 1083 nm atomic line of helium". In: *European Physical Journal D* 21 (2002), pp. 25–55. DOI: 10.1140/epjd/e20020025.

[7] D. Budker et al. "Nonlinear magneto-optical rotation with frequency-modulated light". In: *Physical Review Letters* 85.10 (2000), pp. 2088–2091. DOI: 10.1103/PhysRevLett.85.2088.

[8] P. Gádoros et al. "Laser-induced window cleaning in rubidium vapor cells". In: *Scientific Reports* 12.1 (2022), p. 15530. DOI: 10.1038/s41598-022-19883-0.

[9] NIST. *NIST Atomic Spectra Database Ionization Energies*. https://physics.nist.gov/PhysRefData/ASD/ionEnergy.html. Accessed: 2025-05-08.

[10] W. Gong et al. "Frequency Stabilization of a 1083 nm Fiber Laser to ^{4}He Transition Lines with Optical Heterodyne Saturation Spectroscopies". In: *Review of Scientific Instruments* 85 (2014), p. 073103.

[11] Bernd Kaifler et al. "Measurements of metastable helium in Earth's atmosphere by resonance lidar". In: *Nature Communications* 13 (2022), p. 6042. DOI: 10.1038/s41467-022-33751-6.

[12] Sacher Lasertechnik GmbH. *Helium, D0, D1, D2 1083 nm Metastable Transition*. https://www.sacher-laser.com/applications/overview/absorption_spectroscopy/helium_1083_nm_metastable_transition.html. Accessed: 2025-05-08. n.d.

[13] A. Wojciechowski et al. "Nonlinear Faraday rotation and detection of superposition states in cold atoms". In: *Physical Review A* 81 (2010), p. 033420. DOI: 10.1103/PhysRevA.81.033420.

[14] Wolfgang Demtröder. *Laser Spectroscopy: Basic Concepts and Instrumentation*. 4th. Springer, 2008. ISBN: 9783540749524.

[15] D. Budker et al. "Nonlinear magneto-optical rotation with frequency-modulated light". In: *Physical Review A* 65 (1999), p. 033401.

[16] T. Pan, T. Chen, D. Sun, et al. "Metastable helium Faraday filter for helium lidar to measure the density of the thermosphere". In: *Optics Express* 29.3 (2021), pp. 4431–4439.